Interfacial Phenomena and Heat Transfer, 5(4):251–261 (2017)

EFFECT OF THE SIZE OF DROPLETS ON EVAPORATION

Vladimir Borodulin & Mikhail Nizovtsev*

Kutateladze Institute of Thermophysics, Siberian Branch of the Russian Academy of Sciences, Novosibirsk, 630090, Russia

*Address all correspondence to: Vladimir Borodulin, Kutateladze Institute of Thermophysics, Siberian Branch of the Russian Academy of Sciences, Novosibirsk, 630090, Russia; Tel.: +7 383 316 5336; Fax: +7 383 330 8480, E-mail: v_u_b@mail.ru

Original Manuscript Submitted: 12/11/2017; Final Draft Received: 2/27/2018

In this paper, based on theoretical modeling, the effect of an accommodation coefficient on the evaporation of water droplets is analyzed. Analysis of the influence of convective heat and mass transfer, as well as radiant heat transfer, on the temperature and evaporation time of droplets is carried out. The results of the calculations showed that the accommodation coefficient exerts a weak influence on the evaporation of large millimeter drops. The evaporation time of large droplets varies insignificantly; these droplets have time to cool down to the wet-bulb temperature. The accommodation coefficient strongly affects the evaporation of small submillimeter droplets. These droplets cannot cool down to the wet-bulb temperature during evaporation. It is shown that radiant heat transfer leads to an increase in the droplet temperature during the main evaporation stage and prevents cooling to the wet-bulb temperature. Conversely, convective heat transfer promotes a decrease in the droplet temperature to the wet-bulb temperature.

KEY WORDS: *droplet temperature, evaporation, accommodation coefficient, wet-bulb temperature, diffusion model*

1. INTRODUCTION

Interest in studying the processes of evaporation of liquid droplets is explained by two main reasons. The first reason is the wide variety of natural phenomena in which they are observed. The second reason is the existence of a large number of practical problems in various industries that are associated with these processes (Dhavaleswarapu et al., 2010). In the development of the theory of evaporation, three directions can be distinguished in which the greatest research activity is observed.

One of the earliest directions in the development of the theory of evaporation was in the development of hydrodynamic models. The ideas of J. Stefan on the process of evaporation, as a diffusion process, underlie this direction (Knake and Stranskiy, 1956). The second direction is associated with the development of molecular kinetic models and is based on the study of H. Hertz in relation to the rates of phase change during evaporation (Knake and Stranskiy, 1956). In hydrodynamic models, the laws of conservation of the quantity of matter, momentum, and energy are used to describe evaporation processes in the continuum formulation. In molecular kinetic models, the laws of the statistical kinetics of the motion of molecules are applied. The development of computational technologies has led to the emergence of a third direction of research. This direction is based on direct molecular-dynamic simulation, in which the time history of the positions and the velocities of a set of atoms are predicted using the Newtonian equations of motion (Landry et al., 2007).

Each of the aforementioned approaches has its own set of characteristic spatial and temporal scales, which determines the scope of its application. None of these model approaches can give a complete description of the evaporation of droplets of arbitrary size under different environmental conditions. The approaches that combine the advantages of different models are most perspective. Hydrodynamic models are convenient and widely used to describe the

relatively slow evaporation of large liquid droplets when the environment can be considered as a continuous medium. In the Knudsen layer, which directly adjoins the droplet surface, the basic concepts of a continuous medium lose their meaning and these models become inapplicable. The parameters of the medium in the Knudsen layer can be computed based on molecular kinetic models using approximate solutions to the Boltzmann kinetic equation (Kogan, 1967). Molecular dynamics simulation can be used to study the evaporation of very small droplets whose size is on the order of several nanometers. The models are reconciled with each other through the corresponding boundary conditions at the interfacial surface and outer boundary of the Knudsen layer. Examples of the joint use of hydrodynamic and molecular kinetic models can be found in Young, (1991, 1993); Kortsenshteyn et al. (2012); Luo et al. (2016); and Briones et al. (2012). These models have varying degrees of detail, but they all share a common feature. This feature consists of expanding the range of applicability of purely hydrodynamic evaporation models toward small droplet sizes. Meanwhile, the implementation of calculations of the thermal state of evaporating droplets in each of these models is quite a challenge. It is necessary to develop simpler models that can effectively determine not only the temperature of the droplets and their mass and dimensions during evaporation but can also reveal the physical mechanisms that determine the evaporation of droplets of different sizes.

In this paper, this approach has been developed in the study of the thermal state of evaporating free drops of water of various sizes. The analysis is carried out based on the emission–diffusion model of evaporation of free droplets (Borodulin et al., 2017). The influence of the initial size of the droplets as well as the accommodation coefficient on their evaporation is investigated.

2. GOVERNING EQUATIONS

Assertions and assumptions regarding the emission–diffusion model for evaporation of free droplets are described in detail in Borodulin et al. (2017). In this study, for the convenience of the discussion, its content is briefly formulated. The model considers a free spherical droplet of water placed in air at normal room temperature and humidity. The emission–diffusion model is based on the dynamic balance between the net molecular flux from the interphase surface and molecules transferred into the environment due to convection and diffusion. The net resulting molecular flux of molecules from the interphase surface is determined by the difference between the flux of the molecules emitted by the droplet surface and reflected by the surrounding medium back. The mass flux J_K can be expressed based on the approximate solutions to the molecular kinetic theory through the Hertz–Knudsen–Langmuir, Schrage, Kharangate and Mudawar, (2017), or Young (1991) formulas. The approximate Hertz–Knudsen–Langmuir formula for a planar interphase surface is used in this paper:

$$J_K = \frac{4\pi\gamma R^2}{\sqrt{2\pi \mathrm{R_V}}} \cdot \frac{P_S\,(T)}{\sqrt{T}} \cdot (1-\varphi) \tag{1}$$

where R is the radius of the droplet; T is the absolute temperature of the droplet; γ is the accommodation coefficient; $\mathrm{R_V}$ is the individual gas constant for the vapor; P_S is the saturated vapor pressure; and φ is the relative humidity of the vapor layer near the droplet surface.

The formation of the hydrodynamic flow near the drop occurs at distances of several mean-free paths of vapor molecules far from its surface. Expressions of the vapor mass flux in the hydrodynamic region far from the drop, taking into account the Stefan flow (Fuchs, 1959) and natural convection, can be written as follows:

$$J_H = -2\pi D c_\mu \mu R \cdot \mathrm{Sh} \cdot \ln\left(\frac{1-\varphi\,[P_S\,(T)/c_\mu \mathrm{R_g} T]}{1-\varphi_\infty\,[P_S\,(T_a)/c_\mu \mathrm{R_g} T_a]}\right) \tag{2}$$

where D is the coefficient of molecular diffusion of vapor in the air; μ is the molar mass of the vapor; c_μ is the molar concentration of the vapor–gas mixture; $\mathrm{R_g}$ is the universal gas constant; and φ_∞ and T_a are the relative humidity and absolute ambient temperature at a great distance from the droplet, respectively. The influence of convective mass transfer in Eq. (2) can be taken into account using known relationships between the dimensionless numbers of similarity. Thus, the following dependence of the Sherwood number (Sh) on the Grashof number (Gr) is applied by taking into account the free-convective flow in the model:

$$\mathrm{Sh} = 2 + 0.60\mathrm{Sc}^{1/3}\mathrm{Gr}^{1/4} \tag{3}$$

where Sc is Schmidt number. A diffusion transport occurs at $\mathrm{Sh} = 2$. The Grashof number is determined by the droplet diameter$d$:

$$\mathrm{Gr} = \frac{gd^3\,(T_a - T)}{\nu^2 T_a}$$

where d is the diameter of the droplet; g is acceleration due to Earth's gravity; and ν is the kinematic viscosity of the ambient air.

It should be noted that the expression under the logarithm sign in Eq. (2) is easily expressed in terms of the Spalding mass number $\mathrm{B_m}$ (Spalding, 1956): $1 + \mathrm{B_m}$, where $\mathrm{B_m} = (X_\infty - X_S)/(1 - X_\infty)$, and X is the mole fraction of vapor in the vapor–air mixture. Here, subscripts S and ∞ refer to the interphase surface and ambient air, respectively. The formula for the flow (J_H) acquires the form of Eq. (2) only when the Stefan flow is taken into account. The August–Roche–Magnus formula (Alduchov and Eskridge, 1996) can be used to calculate the saturated water vapor pressure at moderate temperatures from -40°C to $+50$°C. This allows obtaining the value of P_S with a relative error of about 0.4%:

$$P_S\,(T) = 610.94 \cdot \exp\left\{\frac{17.625 \cdot (T - 273.15)}{T - 30.11}\right\}, \quad \Pi a$$

In the model, the equality of flows J_K and J_H is provided by introducing an intermediate vapor layer with relative humidity φ, in which the first boundary is at the interphase surface and the second boundary is at some distance from it, where the hydrodynamic flow has already formed. The unknown value of φ for the intermediate layer is computed using the expression:

$$-2\pi D c_\mu \mu R \cdot \mathrm{Sh} \cdot \ln\left(\frac{1 - \varphi\,[P_S\,(T)/c_\mu \mathrm{R_g} T]}{1 - \varphi_\infty\,[P_S\,(T_a)/c_\mu \mathrm{R_g} T_a]}\right) = \frac{4\pi\gamma R^2}{\sqrt{2\pi \mathrm{R_V}}} \cdot \frac{P_S\,(T)}{\sqrt{T}} \cdot (1 - \varphi) \tag{4}$$

In Eq. (4), the saturated vapor pressure in the layer is taken at droplet temperature T. This assumption is valid for the given case of evaporation of the droplet because the temperature difference at the boundaries of the layer will be small in comparison with the absolute temperature of the droplet.

It is further assumed that the inhomogeneity of the temperature field inside the droplet is small, and it can be considered thermally homogeneous (Sazhin, 2006). The assumption of temperature uniformity of evaporating droplets used in the simulation is valid at low heat and mass transfer rates, when the droplets are at room temperature and humidity. To expand the range of applicability of the model, one can take into account the inhomogeneity of the temperature distribution inside the drop. This will allow more accurate computation of the evaporation rate of moving droplets and droplets exposed to high-temperature gas flow. One of the useful methods that makes it possible to effectively model the temperature inhomogeneity inside the droplet upon evaporation, by taking into account the internal fluid circulation, is the use of the third-order polynomial profile (Zhou et al., 2017).

The rate of droplet evaporation is conveniently expressed in terms of J_K:

$$\frac{dm}{dt} = J_K \tag{5}$$

where m is the mass of the droplet. The droplet temperature T and heat flux q across the droplet surface are computed to determine the thermal state of the droplet during evaporation. The energy conservation law for an evaporating drop can be written as follows:

$$mc^w \frac{dT}{dt} = q + L\,(T_a) \cdot \frac{dm}{dt} + c^w \cdot (T_a - T) \cdot \frac{dm}{dt} \tag{6}$$

Taking into account conductive, convective, and radiative heat transfer, flux q will have the following form:

$$q = 2\pi\lambda_a R \cdot \mathrm{Nu} \cdot (T_a - T) + \pi\varepsilon\,(R) \cdot \sigma R^2 \cdot \left(T_a^4 - T^4\right) \tag{7}$$

where c^w is the heat capacity of water; L is the specific heat of vaporization taken at ambient temperature; ε is the integral emissivity of the droplet surface determined due to the optical properties of water (Zolotarev and Dyomin,

1977) and current size of the droplet; σ is the Stefan–Boltzmann constant; and λ_a is the thermal conductivity coefficient of ambient air. Under conditions of free convection the correlation between the Nusselt number (Nu) and Grashof number (Gr) can be written as follows (Han et al., 2016):

$$\mathrm{Nu} = 2 + 0.60\mathrm{Pr}^{1/3}\mathrm{Gr}^{1/4} \tag{8}$$

A conductive heat transfer with air takes place at $\mathrm{Nu} = 2$. The model also allows one to calculate the evaporation of droplets in the case of forced convection. In this case, to determine the Sh and Nu numbers, it is necessary to use models corresponding to different droplet blowing regimes (Zhou et al., 2013).

The system of equations in Eqs. (4)–(6) allows simulating the evaporation of droplets by taking into account the previously noted limitations. This system can be converted to a dimensionless form through the introduction of a dimensionless value of the temperature and time scale, τ_0:

$$\theta = \frac{T - T_{\mathrm{wb}}}{T_a - T_{\mathrm{wb}}}$$

$$\tau_0 = \frac{\rho_W L R_0^2}{2\lambda_a \cdot (T_a - T_{\mathrm{wb}})}$$

where T_{wb} is the wet-bulb temperature that corresponds to temperature T_a and ambient air relative humidity φ_∞; R_0 is the initial radius of the drop; and ρ_W is the density of the liquid. The evaporation time of the droplet in the Maxwell diffusion model (Fuchs, 1959) is chosen as the time scale τ_0. The mass and radius of the droplet are normalized by their initial values m_0 and R_0. As a result of the substitutions, the system of equations is transformed to the following dimensionless form:

$$\bar{m}\frac{d\theta}{d\bar{t}} = \frac{3}{4}\mathrm{Nu}\cdot\mathrm{K}\cdot\sqrt[3]{\bar{m}}\cdot(1-\theta) + (\mathrm{K}+1-\theta)\cdot\frac{d\bar{m}}{d\bar{t}} + \frac{3}{2}\mathrm{K}\cdot\Lambda\cdot\sqrt[2/3]{\bar{m}}\cdot\Psi(\theta) \tag{9}$$

$$\frac{d\bar{m}}{d\bar{t}} = \frac{3}{2}\mathrm{K}\cdot\frac{\gamma c^w R_0 P_S[T(\theta)]}{\lambda_a\sqrt{2\pi\mathrm{R_V}T(\theta)}}\cdot(1-\varphi) \tag{10}$$

$$\frac{1}{(1-\varphi)}\ln\left(\frac{1-\varphi_\infty[P_S(T_a)/c_\mu\mathrm{R_g}T_a]}{1-\varphi\{P_S[T(\theta)]\}/c_\mu\mathrm{R_g}T(\theta)}\right) = -\frac{2\gamma R_0 P_S[T(\theta)]}{\mu c_\mu D\cdot\mathrm{Sh}\sqrt{2\pi\mathrm{R_V}T(\theta)}}\cdot\sqrt[3]{\bar{m}} \tag{11}$$

where $\mathrm{K} = L/[c^w\cdot(T_a - T_{\mathrm{wb}})]$ is the Kutateladze number; $\Lambda = (\varepsilon\sigma R_0/\lambda_a)\cdot\left(T_a^4 - T_{\mathrm{wb}}^4\right)/(T_a - T_{\mathrm{wb}})$ is the radiation–conduction parameter; and the function $\Psi(\theta) = (1-\theta)\cdot(1+F_1\theta)\cdot\left(1+F_2\theta+F_3\theta^2\right)$ depends on dimensionless temperature θ and the following parameters:

$$F_1 = \frac{(T_a - T_{\mathrm{wb}})}{T_a + T_{\mathrm{wb}}},\quad F_2 = \frac{2T_{\mathrm{wb}}\cdot(T_a - T_{\mathrm{wb}})}{T_a^2 + T_{\mathrm{wb}}^2},\quad F_3 = \frac{(T_a - T_{\mathrm{wb}})^2}{T_a^2 + T_{\mathrm{wb}}^2}$$

The Kutateladze number, radiation–conduction parameter, and numbers F_i are the governing dimensionless parameters for the system of Eqs. (9)–(11). The current value of φ, which regulates the net molecular flux of molecules from the interphase surface, is determined using Eq. (11). The rate of evaporation of the droplet and its current mass is determined using Eq. (10). The new temperature value is then determined from Eq. (9).

Differential Eqs. (9) and (10) were solved numerically by the fifth-order Runge–Kutta–Merson method with correction of the time step at each iteration. Equation (11) was solved by the Newton method. The suggested model was validated by comparison with experimental data obtained by contactless infrared thermography and microphotographing the water droplets at evaporation (Borodulin et al., 2017). Also, the model was validated by comparing the results of the calculations with the results of other models (Wulsten and Lee, 2008). Figure 1 shows the changes in the relative outer surface of the large droplets obtained in the computations using the model and the experiments using microphotography. The experimental data are consistent with the computational results. Figure 1 demonstrates the known linear dependence $(d/d_0)^2$ on time.

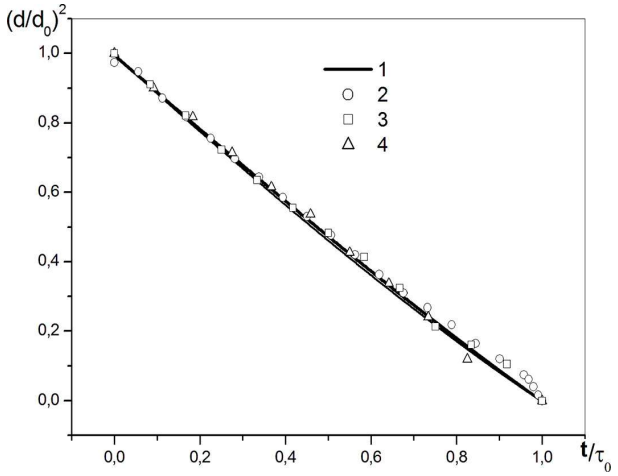

FIG. 1: Outer surface of a droplet as a function of time during evaporation (1, computations: $d_0 = 1$–2 mm; 2, experiment: $d_0 = 1$ mm; 3, experiment: $d_0 = 1.5$ mm; 4, experiment: $d_0 = 2$ mm)

The temperature distribution on the surface of the evaporating droplet was recorded using the infrared thermography method. As a result, the average temperatures of the surfaces of the evaporating water droplets with different diameters d_0 were obtained. Figure 2 presents a comparison of the obtained experimental data and the computational results from the model. From Fig. 2 it may be inferred that the calculation results are consistent with the experimental data. At the initial stage of evaporation, the average temperature of the drops sharply decreased, and then there was an area of relatively constant temperature slightly exceeding the wet-bulb temperature, T_{wb}. At the final stage of evaporation, the theoretical and experimental data showed an increase in the drop temperature. However, the calculation results demonstrated a sharper increase in temperature in the final stage compared with the experimental data, which was probably due to edge effects from the additional heat supply and deviation from the spherical shape of the drops at the end of the evaporation.

3. DISCUSSION OF THE COMPUTATIONAL RESULTS

Before considering the effect of the accommodation coefficient γ on the thermal state of the droplet during its evaporation, some comments should be presented. In this paper, the coefficients of the evaporation and condensation are assumed to be equal. As noted in Marek and Straub (2001), experiments with water give a slight excess in the condensation coefficient in comparison with the evaporation coefficient. However, the scatter of measurement results among different research studies is great. Therefore, in the literature a simplifying assumption about the equality of the coefficients has been made. In accordance with the data from Marek and Straub (2001) and Akulichev (1978) for water at room temperature, the coefficient of accommodation γ is 0.04. A rigorous analysis of coefficient γ was made by Landau (1935). At moderate water temperature, coefficient γ can be estimated by the following expression:

$$\gamma = \frac{1}{6\rho_W \sqrt{2\pi m_m}} \left(\frac{kT}{a^2 c_0^2} \right)^{3/2}$$

where m_m is the mass of the water molecule; k is the Boltzmann's constant; c_0 is the speed of sound in the liquid; and a is the radius of the intermolecular interaction in the liquid. In Akulichev (1978), it was stated that the Landau formula well reflects the functional dependence of the coefficient of accommodation on temperature: $\gamma \sim T^{3/2}$.

In connection with these comments, the question of the degree of influence of the value of γ on the character of the evaporation of droplets becomes topical. Or, in other words, how much will the droplet evaporation time be changed with the changes in the value of γ? What will happen to its temperature? Do these changes depend on the initial size of the droplets? All of the calculations in this paper were carried out under the condition that the initial

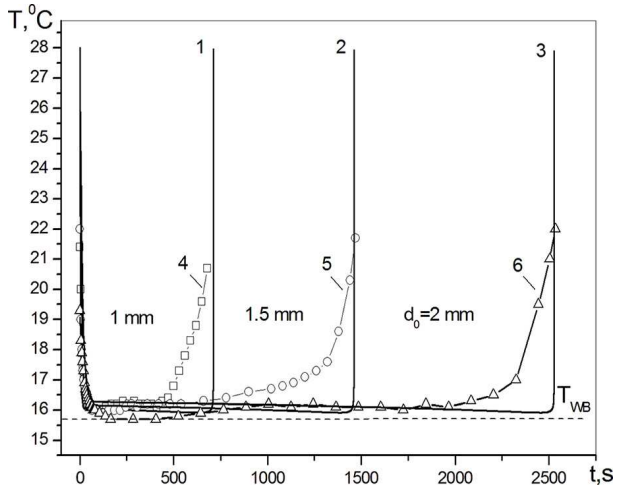

FIG. 2: Comparison of the surface temperature of the drops at evaporation (1, calculation: $d_0 = 1$ mm; 2, calculation: $d_0 = 1.5$ mm; 3, calculation: $d_0 = 2$ mm; 4, experiment: $d_0 = 1$ mm; 5, experiment: $d_0 = 1.5$ mm; 6, experiment: $d_0 = 2$ mm)

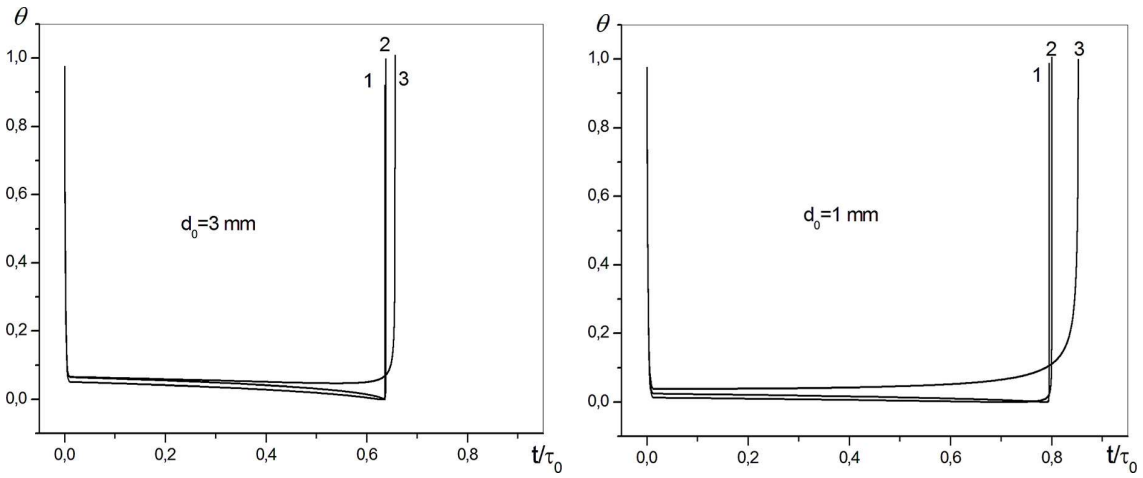

FIG. 3: Dependences of the temperature of large droplets on time for different values of γ (1, $\gamma = 0.4$; 2, $\gamma = 0.04$; 3, $\gamma = 0.004$): (a) the initial diameter of the droplet, $d_0 = 3$ mm; (b) the initial diameter of the droplet, $d_0 = 1$ mm

droplet temperature is equal to the ambient air temperature: $T_0 = T_a$. It was assumed that $T_a = 294$ K, and the relative humidity of ambient air $\varphi_\infty = 50\%$.

Figure 3 shows the dependence of the dimensionless droplet temperature on time. As discussed in Borodulin et al. (2017), at the beginning of evaporation, the droplet temperature decreases sharply from its initial value of $\theta = 1$ to that close to the wet-bulb temperature, $\theta_{wb} = 0$. Then, during a long evaporation time, the droplet temperature changes smoothly. At the end of evaporation, a rapid increase in temperature is observed. The early and final stages of evaporation have a fairly short duration. Mainly, the time of the droplet evaporation is determined by the duration of the long stage with a smooth, slight change in temperature. In the Maxwell diffusion model this stage corresponds to that of adiabatic evaporation, in which the droplet temperature is equal to the wet-bulb temperature.

The decrease in the droplet temperature is due to a phase transition. The rate of change in temperature depends on the thermophysical properties of the liquid and the rate of evaporation. At the initial time, when the droplet and air temperatures are equal, this can be estimated using the expression obtained from Eq. (6):

$$\frac{dT}{dt} = \frac{L\left(T_a\right)}{mc^w}\frac{dm}{dt}$$

Here, the greater the specific heat of vaporization and the smaller the initial heat capacity of the droplet, the greater is the rate of change in the droplet temperature. More precisely, the decrease in temperature occurs relatively sharply in comparison with the time of evaporation of the droplet. For example, as the calculations show, a droplet with an initial diameter $d_0 = 3$ mm cools to a wet thermometer temperature in about 160 seconds, a droplet with $d_0 =$ 1 mm cools in 25 seconds, and a droplet with $d_0 = 100$ μm cools in 0.35 seconds. This is in satisfactory agreement with experimental results (Borodulin et al., 2017).

As can be seen from Fig. 3, the normalized evaporation time depends on the initial size of the droplet. Since the time is normalized by the lifetime of the droplet in the Maxwell diffusion model, without taking into account the Stefan flow, free convection, and radiant heat transfer, the deviation in the dimensionless evaporation time of the droplet from $t/\tau_0 = 1$ characterizes the influence these processes have on evaporation. Figure 3 also shows that free convection and radiant heat transfer exert a greater influence on larger droplets. As shown in Borodulin et al. (2017), with a decrease in the size of the droplets, the role of convection and radiation decreases.

Analysis of the results also shows that changes in γ over a wide range of values have little effect on the evaporation time of large droplets. In the calculations, the accommodation coefficient varied from 0.004 to 0.4. A reduction in γ by a factor of 100 leads to an increase in the evaporation time by only a few percent. Thus, the lifetime of a droplet with $d_0 = 3$ mm increases by about 3%, and with $d_0 = 1$ mm by 7%.

This demonstrates the weak dependence of the evaporation time on accommodation coefficient γ for large droplets in the millimeter range. It should be noted that this effect increases with decreasing droplet size. The most significant deviations in the behavior of the droplet temperature are observed for small γ. As seen from Fig. 3, when $\gamma \geqslant 0.04$ the droplet temperature gradually decreases to the minimum temperature, $\theta_{wb} = 0$. This minimum is achieved immediately prior to intense temperature growth. Another behavior of the temperature is observed for small $\gamma \approx 0.004$. Instead of a gradually decrease in temperature, in the main stage of evaporation growth is observed, which is accelerated at the end of this stage. At the same time, the droplet temperature does not reach the wet-bulb temperature. Of the considered initial droplet sizes, the most significant effect of γ on the droplet temperature change is observed for a smaller size. This trend is more explicit in the submillimeter range of droplet sizes (Fig. 4). For a droplet with $d_0 = 50$ μm, a decrease in γ by a factor of 10 from 0.04 to 0.004 results in an almost twofold increase in the evaporation time (Fig. 4). In addition, there is a significant increase in the droplet temperature deviation from the wet-bulb temperature in comparison with larger droplets (Fig. 3). Therefore, it can be concluded that as the droplet size decreases its sensitivity to a change in the accommodation coefficient rises.

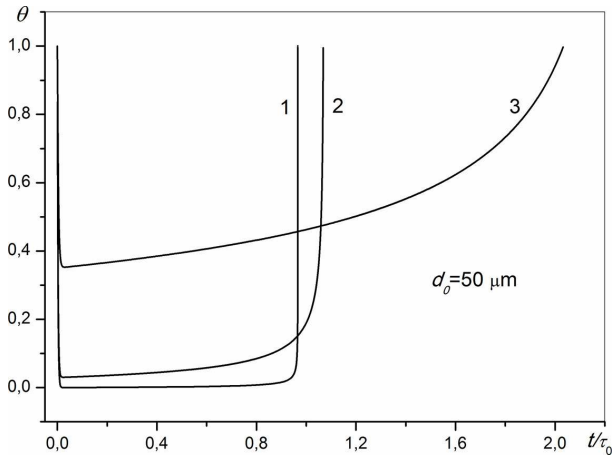

FIG. 4: Dependences of the droplet temperature on time for $d_0 = 50$ μm and different values of γ (1, $\gamma = 0.4$; 2, $\gamma = 0.04$; 3, $\gamma = 0.004$)

Figure 5 demonstrates the effect of the initial droplet size from the submillimeter range on $\theta\,(\bar{t})$ at a fixed value of $\gamma = 0.04$. The relative increase in the evaporation time is characteristic for smaller droplets. The increase in the relative droplet evaporation time for millimeter and submillimeter sizes with the decrease in their initial size is due to different physical mechanisms. For droplets in the millimeter range, this mechanism consists of weakening the role of free-convective and radiant heat transfer with a decrease in their size. For droplets in the submillimeter range, this growth is due to a depleted evaporation regime, when the resulting rate of phase transformations is the determining factor [Eq. (10)].

It should be especially noted that the cause of the increase in the temperature of droplets for the submillimeter range (Figs. 4 and 5), the millimeter range at small γ [Fig. 3(b), curve 3], and finally the millimeter range at the end of evaporation is the depleted evaporation regime (Kozyrev and Sitnikov, 2001). In this regime, evaporation is not determined by mass transfer mechanisms (diffusion, free-convection). The evaporation rate is limited by the net flow of molecules leaving the drop. This flow determines the thermal power during phase transformations, which is in direct proportion to the surface area of the drop, $Q_{PT} \sim R^2$. The power of conductive heat transfer Q_{CD} remains proportional to droplet radius R. Thus, when the droplet evaporates, the heat supply decreases as a function of R, and cooling due to phase changes decreases as a function of R^2. As a result, the heating of the droplet begins to predominate.

It is necessary to analyze the power of the heat fluxes that determine the thermal state of the droplet during evaporation. Figure 6 shows the results of computations for the evaporating droplet with $d_0 = 3$ mm and $d_0 = 50$ μm. Curve (a′ b′ c) shows the change in the power of the conductive heat flux to the droplet, $Q_{CD} = 4\pi\lambda_a R \cdot (T_a - T)$; curve (a′ b‴ c) shows the change in the power of the convective flux, $Q_{CV} = 2\pi\lambda_a\,(\mathrm{Nu} - 2) \cdot (T_a - T)$; and curve (a′ b′^{V} c) shows the change in the power of the radiant flux power, $Q_R = \pi\varepsilon\,(R) \cdot \sigma R^2 \cdot \left(T_a^4 - T^4\right)$. The last two heat fluxes have the same sign and power comparable to the power of the conductive heat transfer. The thermal power, which is spent for the phase transition and heating of the vapor to ambient air temperature, $Q_{PT} = [L\,(T_a) + c^w \cdot (T_a - T)] \cdot (dm/dt)$, is represented by curve (a″ b″ c). As follows from the analysis, for a droplet with $d_0 = 50$ μm, the radiant and free-convective heat flux can be neglected in comparison with the conductive heat flux [Fig. 6(b)]. Since the radiant heat flux is small, adiabatic evaporation is observed, in which all of the supply heat is expended on droplet evaporation. At the initial stage of evaporation [Fig. 6, regions (a′ b′) and (a″ b″)], the power of the conductive heat flux is less than the heat power of the phase transition, as a result, according to Eq. (6) the droplet is cooled:

$$\frac{dT}{dt} = \frac{1}{mc^w}\,(Q_{PT} + Q_{CD}) < 0$$

Radiant and free-convective heat transfer with the environment has a significant effect on the evaporation of relatively large droplets. This effect can be considered in more detail by the example of evaporation of a drop with

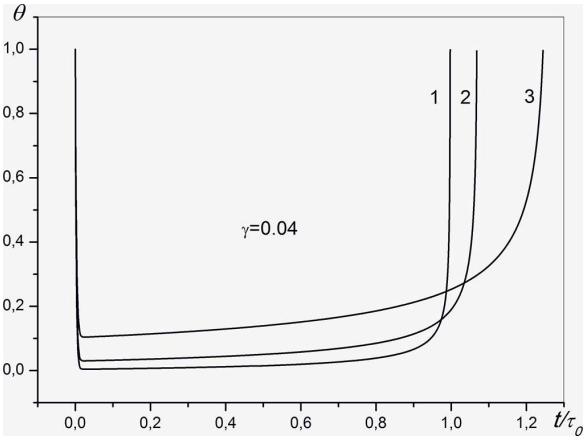

FIG. 5: Dependences of temperature of evaporating droplets on time for different droplet sizes (1, $d_0 = 100$ μm; 2, $d_0 = 50$ μm; 3, $d_0 = 20$ μm) at $\gamma = 0.04$

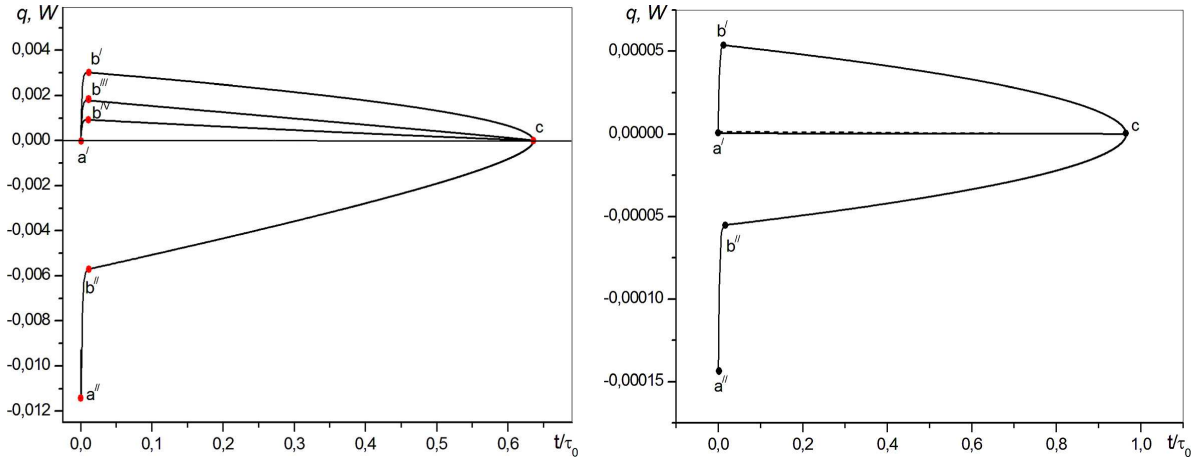

FIG. 6: Dependences of the power of the heat fluxes on time for the evaporating droplet at $\gamma = 0.4$: (a) $d_0 = 3$ mm [curve (a′ b′ c), conductive heat transfer; curve (a′ b‴ c), free-convective heat transfer; curve (a′ b^{V} c), radiant heat transfer; curve (a″ b″ c), phase transition]; (b) $d_0 = 50$ μm [curve (a′ b′ c), conductive heat transfer; curve (a″ b″ c), phase transition]

$d_0 = 3$ mm (Fig. 7). Curve 1 in Fig. 7 corresponds to the conditions when radiant heat transfer and free-convective heat and mass transfer are not taken into account, i.e., $\Lambda = 0$, Nu $= 2$, and Sh $= 2$ [see Eqs. (3) and (8)]. In this case, the evaporation of the droplet and its thermal state are determined by conductive heat transfer between the droplet and environment, the diffusion of the vapor, and the convective Stefan flow, in which the evaporation time is practically equal to τ_0. The droplet temperature for a long interval of the time is nearly the wet-bulb temperature, $\theta_{wb} = 0$. This case differs from the classical Maxwell problem by the presence of the Stefan flow, which has a weak effect on evaporation under these conditions. Curve 2 in Fig. 7 shows the results of the computations, when the influence of radiant heat transfer is taken into account, i.e., $\Lambda \neq 0$, Nu $= 2$, and Sh $= 2$. In this case, the droplet temperature in the main evaporation stage is much higher than θ_{wb}, and the droplet evaporation time becomes less by about 10% due

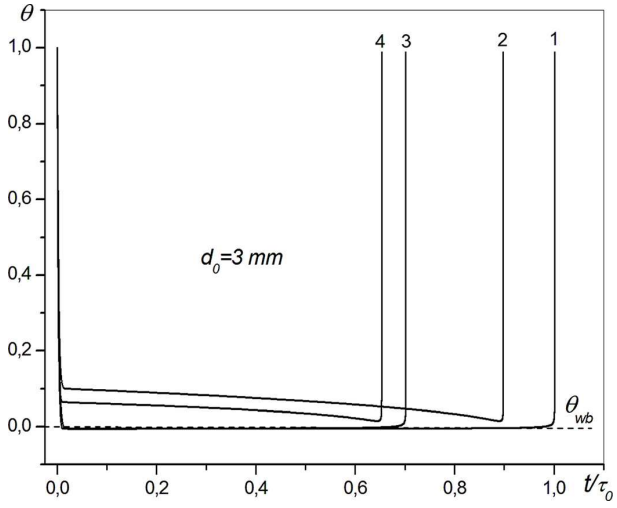

FIG. 7: Dependences of the droplet temperature on time at $d_0 = 3$ mm and $\gamma = 0.04$ (1, without taking into account radiant and free-convective heat transfer; 2, without taking into account free-convective heat transfer; 3, without taking into account radiant heat exchange; 4, with taking into account radiant and free-convective heat transfer)

to the radiant heat transfer. Curve 3 in Fig. 7 shows the results of the computations, when in addition to convection the free-convective heat transfer and mass transfer are taken into account, i.e., $\Lambda = 0$, and the Nu and Sh numbers are determined according to Eqs. (3) and (8). The droplet temperature decreases to θ_{wb}. Evaporation of the droplet occurs more intensively and its evaporation time is reduced by 30% due to free-convective heat transfer. The solution obtained by taking into account all of the mechanisms of the described model is represented by curve 4 in Fig. 7. In this case, the droplet temperature in the main evaporation stage is higher than θ_{wb}, but lower than on curve 2.

The evaporation time decreases by another 5% in comparison with curve 3 (Fig. 7). It should be noted that heat fluxes of radiant and conductive–convective heat transfer [Eq. (7)] increase the internal energy of the droplet. It is clearly seen from the comparison of the curves 2 and 3 in Fig. 7 that the result of their actions is different. At first glance, it would seem that the effect of these heat fluxes on the droplet temperature in the main evaporation stage should be of the same character; however, if the radiant heat transfer is taken into account the droplet temperature becomes higher. Therefore, if free convection is taken into account then there is no such effect. The reason for this contradiction lies in the fact that simultaneously with the intensification of the heat transfer, there is an increase in mass exchange, which is expressed in the model through the Nu and Sh numbers. In this case, the power of heat flux q and the heat power of the phase transitions, $L(T_a) \cdot (dm/dt)$, are the same depending on the droplet size and temperature, but have opposite signs in expression (6). Their mutual compensation occurs when the droplet is cooled to the wet-bulb temperature. In the case of only taking into account the radiant heat transfer the droplet temperature increases directly. As a result, on the main evaporation stage, it turns out that $|q| > |L \cdot \dot{m}|$ and the droplet temperature becomes higher than θ_{wb}. Thus, the radiant heat transfer and convective–conductive heat transfer between the droplet and environment affect the droplet temperature differently.

4. CONCLUSIONS

The analysis of droplet evaporation under the conditions of ordinary room temperatures and air humidity within the emission–diffusion model shows that significant differences in the choice of the accommodation coefficient of water in the range of 0.004–0.4 do not lead to a significant change in the evaporation process and the thermal state of large millimeter droplets. The change in the accommodation coefficient affects the evaporation time of the droplet within a few percent and is most noticeable at the initial and final stages of evaporation. Since the duration of these stages is relatively small, their contribution to the total evaporation time of the droplet is also insignificant. The same weak effect is manifested in the temperature change of large droplets in the main stage of evaporation, and it is characteristic that the influence of the accommodation coefficient is most strong when it decreases relative to the value of 0.04. Therefore, it can be concluded that it is very difficult to accurately determine experimentally the value of the accommodation coefficient when using the value of the evaporation time of large droplets.

The accommodation coefficient has a much more significant effect on the process of evaporation in relation to small submillimeter droplets. The reason lies in the predominance of the role of phase transformations over the processes of mass transfer. The reason that the temperature of large droplets in the main evaporation stage exceeds the wet-bulb temperature is the heat supply due to radiant heat transfer, which does not directly affect mass transfer processes. Intensification of convection simultaneously affects heat transfer and mass transfer, which leads to cooling of the temperature close to the wet-bulb temperature. Thus, these heat supply mechanisms affect the thermal state of the droplet differently during evaporation.

The effect of radiant heat transfer and free convection weakens with a decrease in the size of the droplet during evaporation. In this case, the evaporation is determined by conductive heat transfer, diffusion, and the net molecular flux from the droplet, which depends, among other things, on the accommodation coefficient. Droplets in the submillimeter range cannot cool down to the wet-bulb temperature for the same reason. The smaller the initial size of the droplet, the significantly higher is the minimum temperature to which it can cool.

ACKNOWLEDGMENT

This work was financially supported by the Russian Foundation for Basic Research (Project No. 17-58-53168).

REFERENCES

Alduchov, O.A. and Eskridge, R.E., Improved Magnus Form Approximation of Saturation Vapor Pressure, *J. Appl. Meteorol.*, vol. **35**, pp. 601–609, 1996.

Akulichev, V.A., *Kavitacia v Kriogennyh I Kipiashih Zidkostiah*, Moscow, USSR: Nauka, 1978.

Borodulin, V.Yu., Letushko, V.N., Nizovtsev, M.I., and Sterlyagov, A.N., Determination of Parameters of Heat and Mass Transf. in Evaporating, *Int. J. Heat Mass Transf.*, vol. **109**, pp. 609–618, 2017.

Briones, A.M., Ervin, J.S., Putnam, S.A., Byrd, L.W., and Jones, J.G., A Novel Kinetically-Controlled De-Pinning Model for Evaporating Water Microdroplets, *Int. Commun. Heat Mass Transf.*, vol. **39**, pp. 1311–1319, 2012.

Dhavaleswarapu, H.K., Migliaccio, C.P., Garimella, S.V., and Murthy, J.Y., Experimental Investigation of Evaporation from Low-Contact-Angle Sessile Droplets, *Langmuir*, vol. **26**, no. 2, pp. 880–888, 2010.

Fuchs, N.A., *Evaporation and Droplet Growth in Gaseous Media*, London, UK: Pergamon, 1959.

Han, K., Song, G., Ma, X., and Yang, B., An Experimental and Theoretical Study of the Effect of Suspended Thermocouple on the Single Droplet Evaporation, *Appl. Therm. Eng.*, vol. **101**, pp. 568–575, 2016.

Kharangate, C.R. and Mudawar, I., Review of Computational Studies on Boiling and Condensation, *Int. J. Heat Mass Transf.*, vol. **108**, pp. 1164–1196, 2017.

Knake, O. and Stranskiy, I.N., Evaporation Mechanism, *Prog. Metal Phys.*, vol. **6**, pp. 181–235, 1956.

Kogan, M.N., *Dinamika Razrezhennogo Gaza (Dynamics of Rarefied Gas)*, Moscow, USSR: Nauka, 1967.

Kortsenshteyn, N.M., Samuilov, E.V., and Yastrebov, A.K., Heat Exchange between Phases and Kinetics of Condensation Relaxation for Different Regimes of Droplet Growth, *Colloid J.*, vol. **74**, no. 1, pp. 57–66, 2012.

Kozyrev, A.V. and Sitnikov, A.G., Evaporation of a Spherical Droplet in a Moderate-Pressure Gas, *Phys. Usp.*, vol. **171**, no. 7, pp. 765–774, 2001.

Landau, L.D., Zur Theorie Des Akkommodationskoeffizienten, *Phys. Zeitschr. Sowjetunion*, vol. **8**, p. 489, 1935.

Landry, E.S., Mikkilineni, S., Paharia, M., and McGaughey, A.J.H., Droplet Evaporation: A Molecular Dynamics Investigation, *J. Appl. Phys.*, vol. **102**, p. 124301, 2007.

Luo, X., Fan, Yu., Qin, F., Gui, H., and Liu, J., A New Model for the Processes of Droplet Condensation and Evaporation on Solid Surface, *Int. J. Heat Mass Transf.*, vol. **100**, pp. 208–214, 2016.

Marek, R. and Straub, J., Analysis of the Evaporation Coefficient and the Condensation Coefficient of Water, *Int. J. Heat Mass Transf.*, vol. **44**, pp. 39–53, 2001.

Sazhin, S.S., Advanced Models of Fuel Droplet Heating and Evaporation, *Prog. Energy Combust. Sci.*, vol. **32**, pp. 162–214, 2006.

Spalding, D.B., *Some Fundamentals of Combustion*, London, UK: Pergamon, 1956.

Wulsten, E. and Lee, G., Surface Temperature of Acoustically Levitated Water Microdroplets Measured using Infra-Red Thermography, *Chem. Eng. Sci.*, vol. **63**, pp. 5420–5424, 2008.

Young, J.B., Condensation and Evaporation of Fluid Droplets in a Pure Vapour at Arbitrary Knudsen Number, *Int. J. Heat Mass Transf.*, vol. **34**, pp. 1649–1661, 1991.

Young, J.B., Condensation and Evaporation of Liquid Droplets at Arbitrary Knudsen Number in the Presence of an Inert Gas, *Int. J. Heat Mass Transf.*, vol. **36**, pp. 2941–2956, 1993.

Zhou, Z.-F., Li, W.-Yu., Chen, B., and Wang, G.-X., A 3rd-Order Polynomial Temperature Profile Model for the Heating and Evaporation of Moving Droplets, *Appl. Therm. Eng.*, vol. **110**, pp. 162–170, 2017.

Zhou, Z., Wang, G., Chen, B., Guo, L., and Wang, Y., Evaluation of Evaporation Models for Single Moving Droplet with a High Evaporation Rate, *Powder Technol.*, vol. **240**, pp. 95–102, 2013.

Zolotarev, V.M. and Dyomin, A.V., Optical Constants of Water in Wide Wavelength Range 0.1Å–1 m, *Opt. Spectrosc.*, vol. **43**, no. 23, pp. 271–279, 1977.